ELSEVIER

Polymer 44 (2003) 2721–2738

polymer

www.elsevier.com/locate/polymer

Thermal and morphological properties of main chain liquid crystalline polymers

Bryan B. Sauer*, William G. Kampert, R. Scott McLean

DuPont Central Research and Development, Experimental Station, P.O. Box 80356, Wilmington, DE 19880-0356, USA

Received 11 October 2002; received in revised form 13 January 2003; accepted 14 January 2003

Abstract

Temperature modulated differential scanning calorimetry (TMDSC), variable heating rate DSC, and tapping atomic force microscopy (AFM) were used to study semi-crystalline liquid crystalline polymers (LCPs). Main chain LCPs included a random copolyester (Vectra® A950) and an azomethine alternating copolymer. For the azomethine LCP the TMDSC non-reversing signal detected broad exothermic transitions associated with melting and recrystallization as the slow DSC heating scan induced surprisingly large morphological changes. Non-isothermally crystallized Vectra® and some isothermally crystallized samples at lower temperatures exhibited different levels of DSC scan induced crystal reorganization. Such crystal metastability was also studied by variable heating rate DSC and an independent technique for estimating the melting point at very rapid heating rates. The TMDSC characterization of the scan induced crystal perfection in Vectra® was substantially different than for the other polymers studied. In most cases even though crystal perfection was occurring, no clear exotherm was detected in the non-reversing signal. High temperature annealing for long times resulted in degrees of crystal perfection which could be studied by DSC with minimal scan induced reorganization. High resolution tapping AFM was used to elucidate details of crystal morphology for mechanically oriented and non-oriented Vectra® before and after annealing. Structures resembling lamellae were found to be oriented perpendicular to the chain direction in the oriented Vectra®. In the non-oriented film broad and sometimes curved 'lamellae' were detected. They were about 1000 nm long and between 20 and 35 nm wide, with the width increasing slightly as a function of increased annealing time at 260 °C melt crystallization conditions. Substructure of the lamellae in both oriented and non-oriented Vectra® consisted of smaller stacked crystallites which are detected by AFM studies of these surfaces.

Keywords: Liquid crystalline polymers; Differential scanning calorimetry; Crystallization

1. Introduction

Thermal and mechanical processing histories of main chain wholly aromatic thermotropic liquid crystalline polymers (LCPs) control a variety of crystal morphologies that govern properties [1–5]. LCPs like Vectra® are unique because of the rapid 'solidification' as the crystal network forms in a melt without externally applied stress during cooling [1,2,6–8], followed by various slow crystallization and crystal perfection processes. Because of this rapid solidification into a network where a given LCP chain may span several crystals [9], the chain mobility for further crystallization is severely diminished. So-called secondary crystallization studied in isotropic homopolymers [10–13], would thus be quite different compared to that in LCPs because of larger crystals, chain folding, and other factors in the isotropic systems.

The most widely studied LCPs are random copolymers of 4-hydroxybenzoic acid (HBA) and 2-hydroxy-6-naphthoic acid (HNA), with Vectra® A950 having an approximate ratio of 0.73/0.27, respectively. In Vectra® because of the local chain orientation in the nematic glass, the density difference between crystal and nematic glass phases is very small compared to crystal and glassy phases in isotropic polymers [1,9,14]. Also, the low entropy of melting in thermotropic LCPs causes the high melting points [14], sometimes making the polymer intractable. Melt processable LCPs with lower melting points such as Vectra® are made using comonomers which disrupt the extent of crystallization and crystal perfection [1–4,14–19]. Thermal and morphological studies have shown many common trends for LCP copolyesters containing up to four

* Corresponding author. Tel.: +1-302-695-9705; fax: +1-302-695-8120.

0032-3861/03/$ - see front matter © 2003 Elsevier Science Ltd. All rights reserved.
doi:10.1016/S0032-3861(03)00083-1

comonomers or more [7,20,21]. Most can attain a level of crystallinity of at least 20% especially under solid state polymerization conditions [4,9,16–18]. Much of the work suggests cocrystallization occurs or at least comonomers can be incorporated in the same crystal domains [1,7–9,16,22]. In the case of Vectra® A950, this would consist of some incorporation of the minor component (HNA) into the HBA rich lamellae.

Upon cooling from the melt, the initial crystallization in aromatic polyester LCPs is rapid, and the nature of the slower crystal perfection process ('secondary crystallization') has been widely studied and shows many similarities amongst these various LCP compositions. The Avrami exponents for the fast and slow crystallization regions provide information on the growth mechanism [2,7,8,16]. For the fast crystallization this analysis indicates two-dimensional growth as would be expected for semi-rigid chains in a nematic melt. Kinetic studies by wide angle X-ray diffraction (WAXD) have detected a narrowing of the diffraction lines showing crystal perfection with time [16–18,20]. Several studies have used WAXD to characterize the change in crystal structure as the annealing temperature is increased [6,9,16–18,22,23]. For oriented systems, the diffraction lines are equatorial because of the lateral growth mechanism [1,6,9,17,18]. Many thermal studies of isothermally annealed LCPs have shown consistent results for the slow crystal perfection process where the melting point and heats of fusion increase on a logarithmic time scale [2,7,8,19,20,23–26]. Higher annealing temperatures normally lead to increased rates of change for the slow perfection because of increased mobility or chemical exchange reactions [2,4,7,8,20].

Here we combine temperature modulated differential scanning calorimetry (TMDSC), variable heating rate DSC, and atomic force microscopy (AFM) to investigate the morphological development in Vectra® A950 and another main chain LCP homopolymer. The combination of techniques including an independent rapid heating rate technique for determining melting points without DSC scan induced recrystallization effects, provides new understanding of the thermal and morphological properties of these systems. Previous TMDSC studies of the crystal to nematic transition and nematic liquid-to-isotropic liquid transition have provided background for the application of TMDSC to LCPs [27,28].

2. Experimental

2.1. Materials

Vectra® A950 is a semi-crystalline random copolyester of 4-hydroxybenzoic acid (HBA) and 2-hydroxy-6-napthoic acid (HNA) with a monomer ratio of 73/27. The azomethine LCP is an alternating copolymer with the structure and thermal properties given previously [21,29]. Scheme 1 shows the structure with a flexible polymethylene spacer of seven methylene units connected to the rigid azomethine unit by ether linkages. The polymer was prepared from terephthaldehyde and 1,7 bis(4-amino-3-methyl phenoxy) heptane as reported previously [29].

The respective powders were melted to make thin polymer films 2–5 mg in weight. Cold crystallized samples were prepared by heating to the desired annealing temperature at ~500 °C/min by pressing into a small temperature controlled brass chamber with N_2 flow. For melt crystallization, after melting at 340 °C for 2 min on a hot plate, the sample was quenched into the small brass chamber at the annealing temperature for the desired time. After melting at 340 °C for 2 min in the DSC cell, samples were also cooled in the DSC cell to the desired annealing temperature at 20 °C/min. After annealing they were quenched to room temperature at ~500 °C/min. Cold crystallization refers to heating the sample from the glassy state at room temperature to the crystallization temperature, and melt crystallization refers to cooling from the melt to the isothermal annealing temperature. Most of the isothermally annealed Vectra® samples were melt crystallized.

2.2. Methods

A TA Instruments (New Castle, DE) 2920 DSC was used in these experiments. TMDSC underlying heating rates of 2 or 3.5 °C/min were typically used with a modulation amplitude of the sinusoidally varying temperature of 0.32 and 0.56 °C, respectively, with a period of 60 s based upon the recommended specifications [30] to obtain 'heating only' modulated temperature profiles. The modulation temperature amplitude is relatively small so there is no local cooling during the standard TMDSC scan. This is referred to as a heating-only temperature modulation profile. Data analysis software was supplied by the manufacturer [31]. DSC was also performed at heating rates between 1 and 50 °C/min. An N_2 purge was used for all experiments. Baseline calibration was performed regularly at the different heating rates [32]. Other calibrations were the same as reported previously [32]. Literature has shown [33] that with most polymers, thin and small (~2–3 mg) films and 1 or 2 °C/min underlying heating rates with heating only profiles will result in linearity of the heat flow response. Previously [32], we presented many control experiments with different sample sizes, thicknesses, modulation periods, and heating rates, to address linearity.

In TMDSC, Total = reversing (R) + non-reversing (NR). Differences in total, R, and NR signals due to variations of underlying heating rate are important. For example, the extent of recrystallization can be affected by underlying heating rate and this is a parameter that actually influences the physical state of the sample and is addressed later. Toda et al. [34] have obtained TMDSC data as a function of the temperature modulation period. They have

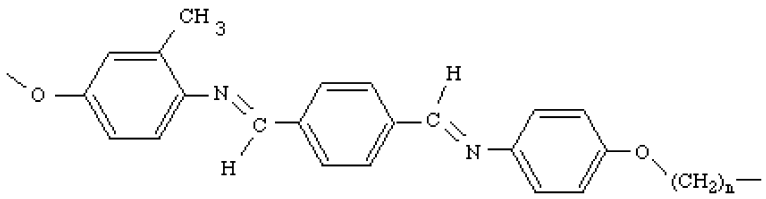

Scheme 1. Structure of azomethine LCP ($n = 7$).

used a model that considers how this modulation frequency affects time constants for melting which vary with temperature through the melting region in PET and other materials, and have shown that this is an important variable that modifies the experimental data as a function of modulation period for typical semi-crystalline polymers.

2.3. Interpretation of TMDSC

We are mostly concerned with interpretation of typical TMDSC heating scans [32,35,36]. The NR signal detects all heat flow in the calorimeter that is not in phase with the modulated temperature; i.e. the heat flow that is insensitive to the experimental temperature modulation in TMDSC. Because the kinetics of crystallization are inherently slow, crystallization events are detected in the NR signal and not the reversing signal. In the TMDSC NR signal, the heat flow component is not affected by the temperature modulation. For example, if melting kinetics become so slow enough that the melting is insensitive to the experimental temperature modulation, then such processes will contribute to the NR endotherm [37,38]. This can also be assessed by examining the raw modulated heat flow data. We typically check the modulated heat flow profiles and verify that the zero heating rate points on each cycle are consistent with the calculated NR data [37,38]. One common example of a NR endothermic contribution is melting of superheatable crystals [11,35,38].

The TMDSC reversing endothermic signal detects melting processes that are in phase with the modulated temperature [39–41]. During modulation, as the rate of temperature increase slows and approaches isothermal, the rate of melting slows and becomes approximately zero for a completely reversing melting process. The glass transitions are also separated entirely into the reversing signal, as are nematic-to-isotropic liquid crystalline or LCP transitions as was demonstrated in recent studies [27,28].

2.4. Rapid heating rate melting point determination

To measure the melting properties of crystals originally present in the sample at heating rates fast enough to avoid recrystallization, a ~2 mg section of the sample is quickly pressed against a temperature controlled metal surface using a procedure described previously [32,35]. As the metal surface temperature is varied, one polymer 'particle' must be used for each temperature to prevent elevated temperature recrystallization, so it is somewhat tedious to vary the temperature and measure these melting points at very high heating rates. Examination of liquid-like flow in these rapidly heated specimens is part of the criteria. In the case of Vectra®, the liquefied samples are also tested by attempting to quickly draw fibers after apparent melting occurs. If fine diameter fibers are readily drawn this establishes true liquid flow. In the cases of gel behavior or even paste like 'flow' under applied force, the samples were considered to be incompletely melted. One expects that such a measurement if done properly will measure the melting of primary crystals originally present in the sample without reorganization contributions. This rapid heating rate melting point method gives melting points designated $T_{m,rapid}$.

2.5. AFM

AFM was performed using tapping mode* (Nanoscope 3A, Velco, Co., Santa Barbara, CA) in air, using methods described previously [42]. Very sharp micro-fabricated tips (Velco, Santa Barbara, CA) with 6–10 nm radii of curvature were used. The tip is oscillated normal to the surface and as the tip is engaged on the surface the height data are measured by a feedback loop where the vertical distance is adjusted to keep the tip oscillation amplitude constant. Simultaneously the phase lag is measured between the tip driving signal and the actual tip response. These 'phase' data are sensitive to local stiffness differences of species or domains near the surface [42–44]. We use 'moderate force' tapping where the free air oscillation amplitude is reduced by about 40% upon engagement of the tip with the surface, as is discussed in previous work [42]. Under these 'moderate tapping force' conditions, hard domains have a larger phase lag [42–44] which is plotted as light regions.

Films were prepared on glass slides and crystallized with the appropriate thermal history. Oriented Vectra® filaments were also studied here, and several images from three different filaments were taken at various spots on the surface to ensure reproducibility.

3. Results

Crystallization and crystal perfection in LCPs has been studied by a variety of techniques. Most of the studies have been performed on HBA/HNA copolymers related to Vectra® A950 including some studies on oligomeric and

low MW HBA/HNA copolymers [17,18]. Many studies using wide angle X-ray scattering methods were applied to oriented LCP systems [1,6,9,17,18]. Annealing of these oriented systems generally contributed to perfection of crystals as was characterized by sharpening of WAXD and small angle X-ray peaks. We have chosen several thermal histories for the thermal studies. For the first few AFM morphology studies presented here (Figs. 1–3), we have prepared oriented monofilaments using procedures similar to those applied by Windle and coworkers [17]. These were studied by AFM before and after annealing at 230 °C for 1 h. Before annealing a very fine crystal morphology is detected with relatively low contrast between crystal and non-crystalline regions (Fig. 1), and after annealing the crystal morphology becomes perfected with a well known orientation of 'lamellae' perpendicular to the fiber direction (Fig. 2) [9,17]. The contrast between crystal and non-crystalline regions also increases substantially, partly because the crystals seem to protrude out of the surface. For the unannealed sample some orientation of structures can be perceived. Some of the faint structures are presumably due to the imperfect crystals which rapidly lock chains into a network during rapid crystallization and network formation [9]. Previous AFM studies of extruded and oriented thick films also provided detailed characterization of fibril structure at the surface [45]. Our AFM results are consistent with several models where imperfect crystals form by lateral registration of crystallizable groups where the chains are oriented before crystallization starts. One chain can span several crystals contributing to the unusual crystal morphology and lack of mobility for further crystallization [9]. Upon annealing, crystal lateral perfection occurs perpendicular to the orientation direction (Fig. 2) [9,17].

In a way, AFM provides a better understanding of the relative fractions of crystal and non-crystalline regions than TEM of etched surfaces. Etching selectively removes non-crystalline material making the crystalline fraction appear greater. In AFM one assumes the bulk morphology is similar to the surface, and AFM also suffers from the fact that its finite probe depth of about 10 nm leads to exaggerated levels of crystals at the surface relative to the bulk in some systems [42].

In Fig. 2 the long period or spacing between lamellae perpendicular to their long direction is 45 ± 10 nm, with the lamellae 50–100 nm long and 12–16 nm thick. Using the molecular weight of 38,000 g/mol and chain length of 200 nm given by Hudson, et al. [9] the lamellar thickness of 14 nm correspondence to about 19 monomer repeats considering the average composition of the copolymer. The long period is consistent with values determined by SAXS for similarly prepared low molecular weight HBA/HNA copolymers. [18] The lamellae are comprised of small crystallites. These small crystallites are approximately 10 nm thick and 15 nm long in the oriented sample (Fig. 2), and are oriented with their long direction perpendicular to the lamellae. Although at the surface these small crystallites which comprise the broader lamellae look separate, there is no way to know with AFM whether the crystallites are connected underneath. Fig. 3 is a lower magnification AFM image showing lamellar orientation and other features related to the smaller crystallites which merge to form lamellae.

Boundaries between macro-fibrils formed during our fiber drawing process are seen in both topography and phase near the bottom of Fig. 2 with only slight disruptions of lamellar orientation at the boundary. Typical diameters are 0.5–3 μm and the fibrils are not well resolved but are detected mostly in the AFM height data [45]. Shear and elongation stresses are known to contribute to the hierarchical arrangement including macro-fibrils in LCPs.

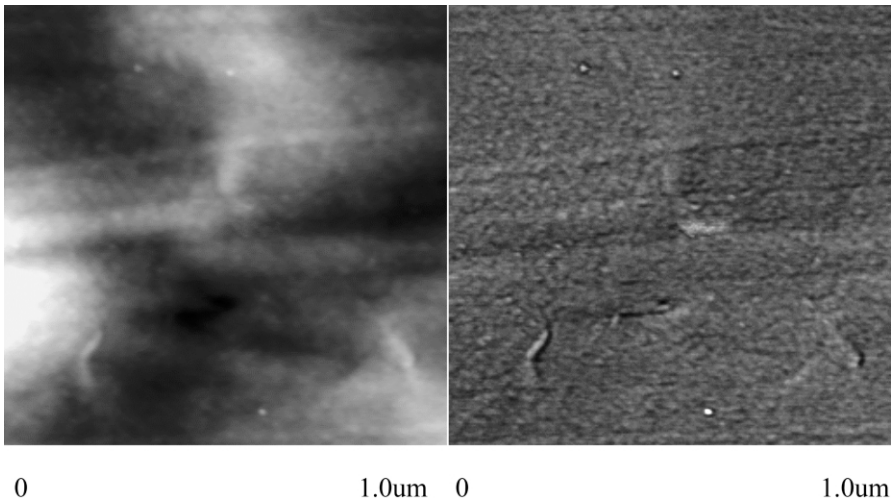

Fig. 1. AFM moderate tapping force height (left) and phase (right) data for a non-isothermally crystallized and oriented Vectra® mono-filament surface. White are high phase corresponding to hard domains. Phase data characterize the imperfect crystal network structure where individual crystals are small and lack contrast. Some indication of structures aligned in the orientation direction is seen. Scan boxes are 1000 nm × 1000 nm for each plot, and *z*-scales are 0–20 nm and 0–15°, respectively. Orientation direction is close to horizontal.

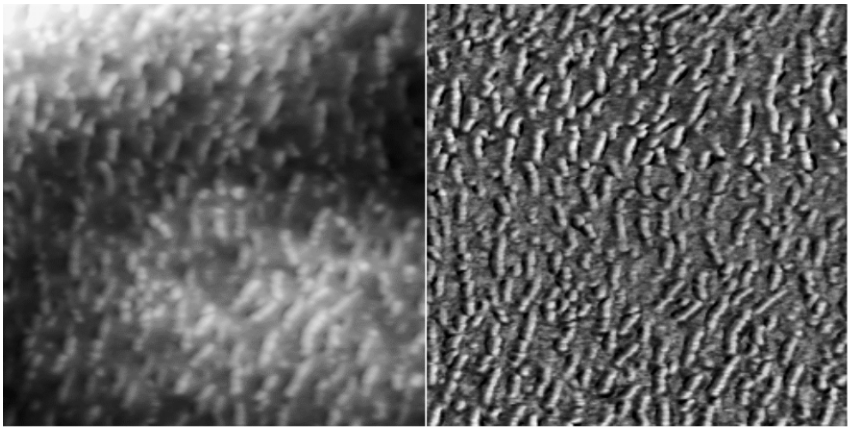

Fig. 2. AFM moderate tapping force height (left) and phase (right) data for the oriented Vectra® mono-filament after cold crystallization at 230 °C for 60 min. White are high phase corresponding to hard domains. Height and phase data resolve perfected lamellae with their long dimension oriented perpendicular to the fiber orientation direction. The lamellae are composed of smaller units in these images suggesting that coalescence of smaller crystals is partly responsible for lateral perfection of lamellae. Scan boxes are 1000 nm × 1000 nm for each plot, and z-scales are 0–50 nm and 0–20°, respectively. Orientation direction is close to horizontal.

Although oriented Vectra®-like systems crystallized at various temperatures show substantial changes in morphology and have been relatively well characterized by electron microscopy [17], electron microscopy studies of isotropic Vectra® and related polymers are rare [9]. A non-oriented Vectra® film with one surface contacting a glass slide and the other contacting air was cooled from the melt at 350 °C to room temperature at − 20 °C/min. The crystallization was rapid during cooling and occurred starting at around 230 °C [2]. Broad and sometimes curved lamellae were detected in the AFM images (Fig. 4). As with the oriented system, the lamellae are comprised of small crystallites. They are about 7 nm × 20 nm in dimension and oriented with their long direction perpendicular to the lamellae. Such crystallites may be even smaller than the dimensions given above because of tip broadening artifacts for such fine features. The repeat period in the direction perpendicular to the long direction of the small crystallites is 25 ± 4 nm, and the repeat distance of the lamellae in the direction perpendicular to the long direction of the broad lamellae is about 70 nm. From examination of the lamellar orientation versus chain orientation in the oriented mono-filament, we can infer that the chain orientation is perpendicular to the long direction of the large lamellae in these isotropic systems. Even though WAXD characterizes quenched samples to be approximately 28% crystalline [9], AFM images of quenched films show essentially no organized structures with just barely resolvable crystallites and no hint of organization into lamellae (not shown here).

Fig. 4B provides lower magnification images where the arrangements of lamellae are seen in more detail. At the bottom of Fig. 4B, relatively large regions of parallel

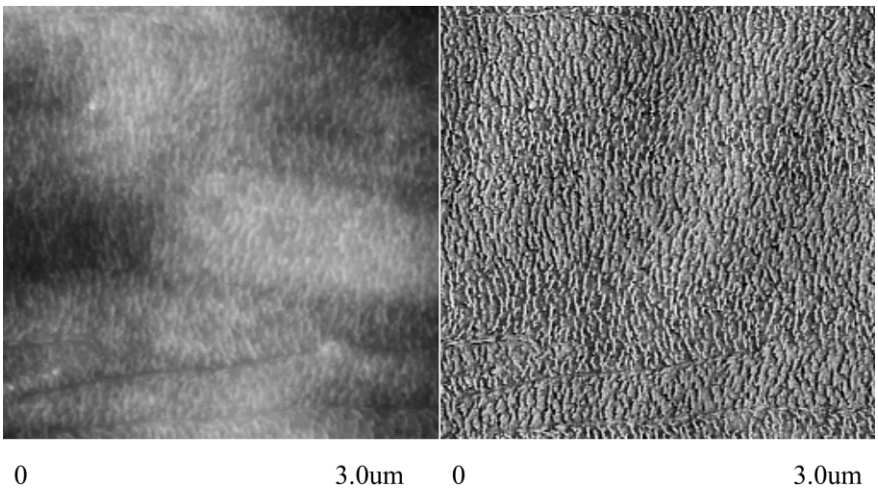

Fig. 3. Lower magnification AFM moderate tapping force height (left) and phase (right) data for the oriented Vectra® mono-filament after cold crystallization at 230 °C for 60 min. Scan boxes are 3000 nm × 3000 nm for each plot, and z-scales are 0–100 nm and 0–20°, respectively. Orientation direction is close to horizontal.

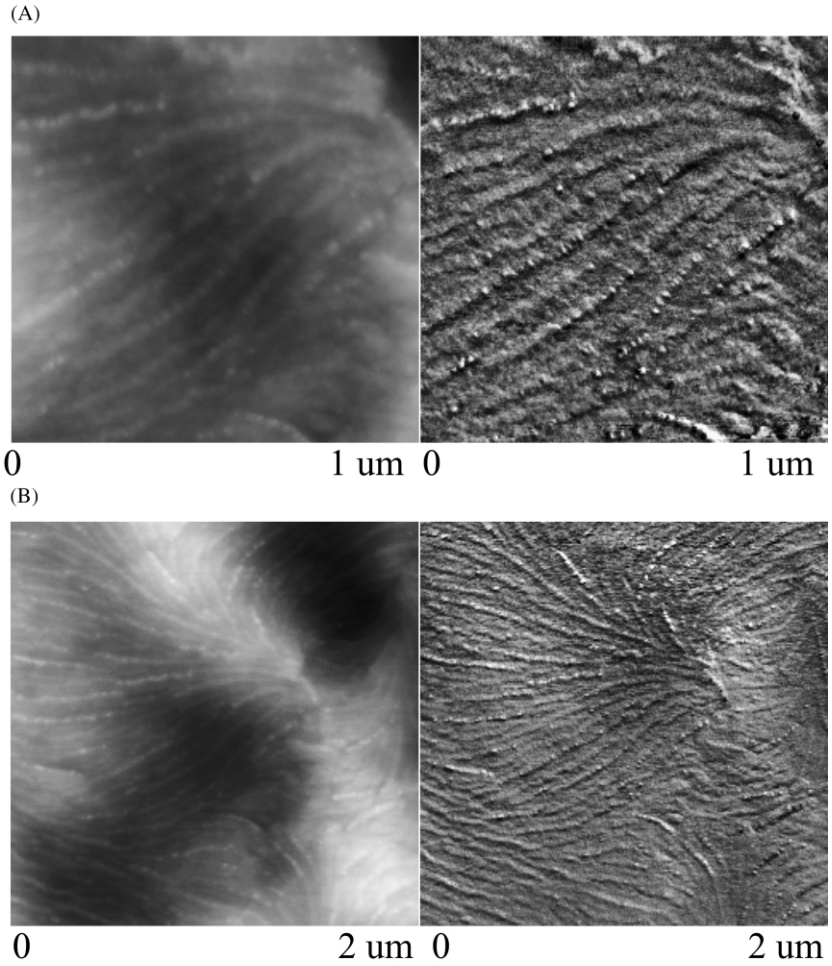

Fig. 4. AFM moderate tapping force height (left) and phase (right) data for a non-isothermally crystallized non-oriented Vectra® film surface. Scan boxes are 1000 nm × 1000 nm (top two images), and 2000 nm × 2000 nm (bottom two images). *Z*-scales are 0–50 nm for height data and 0–10° (top) and 0–20° (bottom) for phase data.

lamellae form presumably as a result of the parallel chain orientation in the nematic melt. To the right of the center of the image, other effects due to disclinations and grain boundaries are seen consistent with some previous characterization [9].

Isothermally melt crystallized samples were prepared by heating to 350 °C for 1 min, cooling at −100 °C/min to 252 °C, and holding isothermally for 10, 130, and 1000 min before quenching to room temperature for AFM analysis. The high magnification image for the 10 min annealed Vectra® film surface in Fig. 5 shows a few lamellae more than one micron long, again composed of strings of much smaller perpendicularly oriented and stacked ca. 11 nm thick and 24 nm long crystallites. In some areas these crystallites are well resolved, and in other regions they are not resolved and seem to partly merge. The lower magnification images of this sample are given in Fig. 6A, showing sometimes strong curvature of the lamellae in both height and phase data. Further annealing of the sample for total of 130 min at 252 °C, gives similar lamellae (Fig. 6B). The main difference between 10 and 130 min of annealing is the higher number of lamellae per unit area for the longer time and a slight increase in thickness and width of the small crystallites. The density of lamellae and crystallites at the surface of the non-isothermally crystallized sample in Fig. 4 is much higher than these isothermally melt crystallized films (Figs. 5 and 6). This is presumably due to the higher undercooling (lower temperature of crystallization) leading to a higher nucleation density in the former system. Fig. 6 also shows that the small crystallites are still present and aggregate to form lamellae. Further annealing at 252 °C for 1000 min led to negligible changes in the dimensions of the lamellae (not shown here), and most of the morphological features are quite similar to those in Fig. 6B. The main difference was poorer contrast between non-crystalline and crystalline phases, suggesting a hardening of the non-crystalline phase after 1000 min.

3.1. TMDSC of azomethine LCP

The total heat flow curve at 3.5 °C/min for the azomethine sample prepared by non-isothermal cooling from the melt at 20 °C/min is given in the top of Fig. 7. The glass transition at 43 °C is followed by a cold crystallization

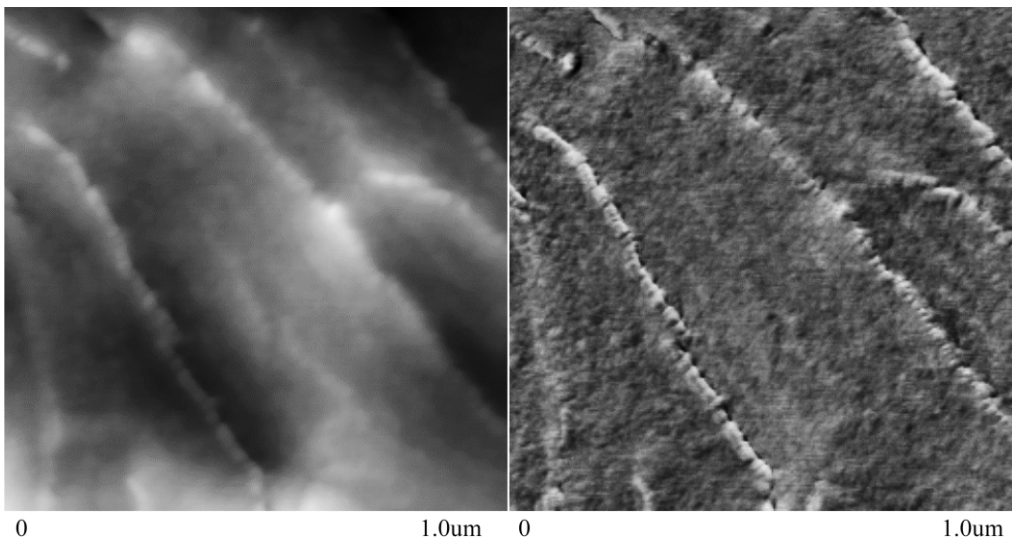

Fig. 5. AFM moderate tapping force height (left) and phase (right) data for an isothermally melt crystallized (252 °C, 10 min) non-oriented Vectra® film surface. Scan boxes are 1000 nm × 1000 nm. *Z*-scales are 0–50 nm and 0–30°, respectively.

exotherm at 97 °C with a ΔH of 14.5 J/g. A double endotherm is characterized by two local minima at 141 and 163 °C and a combined ΔH of 18.2 J/g. This region is the transition from a semi-crystalline nematic-to-nematic liquid (C ⇒ N) as reported elsewhere [21,29]. The highest endotherm at 309 °C is the nematic-to-isotropic transition or clearing point and has a ΔH of 11.6 J/g. Integration of the total heat flow over the entire temperature range gives an endothermic response of 15.3 J/g.

Higher heating rate DSC data were obtained (40 °C/min) and is displayed above the 3.5 °C/min scan in Fig. 7. The total heat flow data show a cold crystallization peak at 123.3 °C with a heat of crystallization of 5.5 J/g. Next, a single peak endotherm of 6 J/g is detected at 160 °C which is the melting of these just formed crystals. Finally, the nematic to isotropic transition occurs at 309.5 °C with a heat of fusion of 10.3 J/g.

The reversing heat flow detects the glass transition at 44 °C, a double melting endotherm at 142 and 162.5 °C, and then a final endothermic transition at 309.4 °C (Fig. 7). The

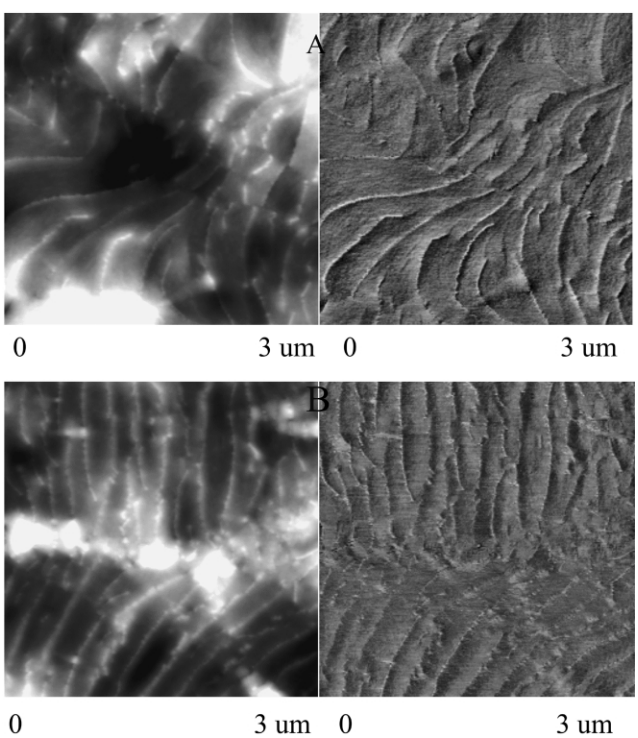

Fig. 6. Lower magnification AFM moderate tapping force height (left) and phase (right) data for an isothermally melt crystallized non-oriented Vectra®. Upper two images are 252 °C, 10 min, and lower two images are 252 °C, 130 min. All scan boxes are 3000 nm × 3000 nm. *Z*-scales are 0–50 nm (left) and 0–25° (right), respectively.

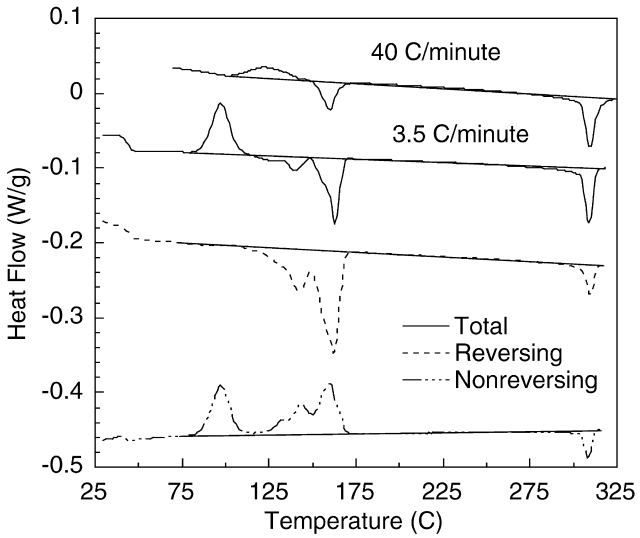

Fig. 7. Total (solid), reversing (dash) and non-reversing (dot-dash) TMDSC data with a 3.5 °C/min heating rate for the Azomethine LCP. The total (solid) heat flow for a 40 °C/min experiment is at the top and has been scaled by heating rate. The curves have been shifted vertically for clarity. The total signal is the sum of the R and NR signals and is equivalent to a standard DSC curve.

melting processes below 162 °C involves the various mesomorphic crystal transformations and the C ⇒ N transition. The region has a total heat of fusion of 44 J/g. The final endothermic signal represents the nematic-to-isotropic liquid transition [29] or clearing point and has a reversing ΔH of 5.6 J/g.

The total heat flow minus the reversing heat flow gives the NR heat flow. All exothermic behavior is separated into this signal, in addition to endothermic melting in some cases (see Section 2). A 'cold crystallization' exotherm is detected at 97 °C and has a ΔH of 15 J/g (Fig. 7). The cold crystallization is followed by a transition region which shows a reorganization/reperfection process with substantial NR exothermic behavior from 125 to 180 °C and an integrated ΔH of 25 J/g over this region. This exotherm has three peaks at 132.4, 143.4, and 160.2 °C with the highest having the largest peak area. The clearing point or nematic-to-isotropic transition has a peak temperature of 308.4 °C and a ΔH of 3.2 J/g.

The substantial complexity of TMDSC in the study of semi-crystalline polymers has been widely discussed in the literature [34,38–41]. To more fully understand the TMDSC technique, the region between 50 and 200 °C is expanded and includes the C ⇒ N transition at 162 °C (Fig. 8). Four curves are displayed including total, reversing, non-reversing, and raw modulated heat flow profiles. The modulated heat flow (solid line) represents the calorimeter response to the imposed oscillating temperature. The moving average of the raw modulated heat flow signal is calculated [31] and this provides the total heat flow. The temperature of the peaks of the processed curves (R and NR) are slightly shifted toward higher temperatures compared to analogous transitions in the modulated heat flow data by

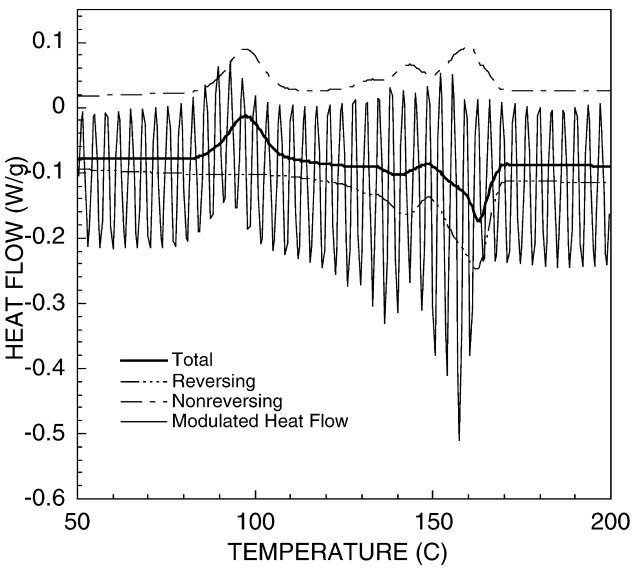

Fig. 8. Total (thick solid), reversing (dot-dot-dot-dash), non-reversing (dot-dash), and modulated heat flow (solid) TMDSC data with a 3.5 °C/min heating rate for Azomethine. The curves have been plotted on the same overall scale.

about 1.5 cycles due to the 'real-time' deconvolution (Fig. 8) [31]. The zero heating rate portion of each modulated heat flow cycle corresponds to the peak maximum of each cycle in Fig. 8, and these maxima should roughly map out the calculated NR curve given the 1.5 cycle temperature displacement.

Visual checks of the quality of the TMDSC experiment can be accessed in part by key aspects of the raw heat flow profile. In a modulated experiment, one must check for adequate cycles through thermal transitions. It is desirable to have four modulation periods over the temperature range of each transition studied. In this data set, there is a sufficient number through the cold crystallization exotherm at 97 °C and the highest reversing endotherm at 162.5 °C (Fig. 8). However, the slightly lower temperature reversing endotherm at 142 °C is questionable, as is the sharp 309 °C transition. An experiment was also run using an underlying heating rate of 1 °C/min and a 100 s modulation period through the 309 °C transition region giving approximately the same results in terms of the separation into R and NR components. We performed this to ensure sufficient number of modulation cycles through the transition [31], and to confirm linearity by pushing toward lower instantaneous heating rates in the modulated temperature program. In these TMDSC experiments, the relative fraction of R and NR was approximately the same.

Chen, et al. [27,28] have shown the expected reversibility and independence of the nematic-to-isotropic transition temperature on heating and cooling in a different LCP. This transition was also about an order of magnitude narrower than that in our azomethine LCP. For our azomethine LCP, heating, cooling, and then heating again at 10 °C/min showed about 5 °C hysteresis in the DSC peak temperatures. It is possible that the kinetics are such that they govern both the hysteresis and the rather large NR component for this 309 °C transition. There was also some thermal instability of the azomethine LCP if annealed for minutes at 320 °C. This caused a dramatic lowering and broadening of the nematic-to-isotropic transition and could affect the TMDSC characterization of this transition even in situations where no substantial degradation was detected.

3.2. TMDSC study of non-isothermally crystallized Vectra®

A Vectra® sample was heated to 340 °C for 5 min to erase any prior thermal history, and cooled to room temperature at ~20 °C/min. A TMDSC experiment on a ~4 mg sample was performed at 3.5 °C/min. The total heat flow curve shows a broad glass transition followed by double endothermic melting (Fig. 9). The peak temperatures are 278.9 and 294 °C and the total integrated heat of fusion is 5.8 J/g. The $T_{m,rapid}$ of this sample is 260 °C and was measured as described in Section 2. This value of $T_{m,rapid}$ is illustrated by the vertical line in Fig. 9 and will be discussed in more detail later.

The reversing signal will be described first. The glass

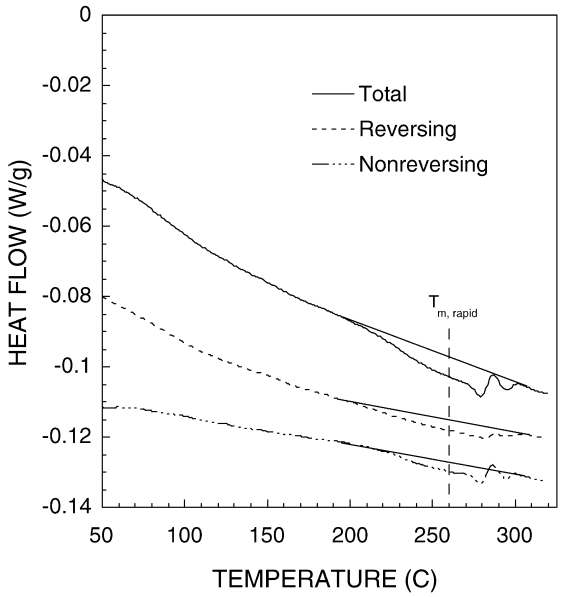

Fig. 9. Total (solid), reversing (dash) and non-reversing (dot-dash) curves at 3.5 °C/min for non-isothermally crystallized Vectra®. The curves have been shifted vertically for clarity. The rapid heating rate determination of the melting of species 'originally' present is $T_{m,rapid} = 260$ °C and is indicated by the dashed vertical line (see text).

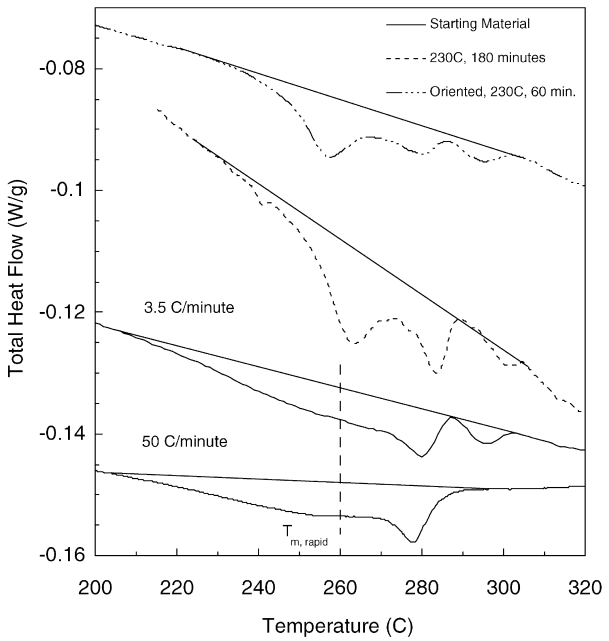

Fig. 10. Total heat flow curves of non-isothermally crystallized Vectra® ('starting material') at 3.5 and 50 °C/min (solid curves). Subsequent annealing is indicated by a dashed curve for a sample that was cold crystallized at 230 °C for 180 min. Also, total heat flow (dot-dash) curve of TMDSC data at a 3.5 °C/min heating rate for an oriented sample cold crystallized at 230 °C for 60 min. The curves have been shifted vertically for clarity. The rapid heating rate determination of the melting of species originally present in the non-isothermally crystallized sample (termed starting material) equals 260 °C and is indicated by the dashed vertical line.

transition is detected in the reversing signal only, with an onset and end at ~74 and ~98 °C, respectively. The midpoint is 86 °C with a ΔC_p of 0.054 J g^{-1} K^{-1}. Under this and most other crystallization conditions for Vectra®, a nematic mesophase with a degree of crystallinity and a high surface area crystal morphology restricts the ability of the chains to contribute to the glass transition. A weak double melting peak is detected in the reversing curve. This melting process starts ~200 °C and ends around 300 °C with peak temperatures of 281.8 and 295.8 °C. The integrated heat of fusion for the reversing curve is 3.2 J/g.

The NR curve in Fig. 9 shows a broad endothermic melting process starting at 200 °C with a broad transition before the sharper minimum at 278.9 °C. This is immediately followed by a rise in the baseline to an exothermic peak of 286 °C, and a small melting process with a endothermic peak minimum at 295 °C. The integrated heat of fusion for the non-reversing curve is 2.6 J/g. The NR curve is interpreted by considering the lower endotherm region to consist of a sequence including the melting of the 'primary' species at lower temperatures (200 and 280 °C), followed by a small exothermic peak due to recrystallization at 286 °C, and the small high temperature endotherm due to melting of these recrystallized species. The broad lower melting region between 200 and 280 °C is complex because of various scan induced reorganization effects discussed in more detail below. At higher scan rates, the exotherm and 295 °C endotherm vanish proving that they are due to recrystallization and have some similarities to crystallized PET (Fig. 10).

Because annealing had such a dramatic effect on lamellar development in the AFM results in Fig. 2, efforts at perfecting the morphologies of various non-isothermally crystallized (N-IC) samples will be described. Total curves at 3.5 °C/min are given in Fig. 10 for the N-IC sample with no additional annealing, a N-IC sample further cold crystallized at 230 °C for 180 min, and an oriented sample cold crystallized at 230 °C for 60 min. After 180 min the 'secondary' melting endotherm at 263 °C becomes much stronger relative to the original N-IC sample. A 50 °C/min scan was also performed on the N-IC sample to confirm the suppression of part of the reperfection process and is displayed below the 3.5 °C/min curve in Fig. 10. For the 230 °C annealed oriented sample, the lower endotherm at 256.8 °C is well developed, but the higher endotherms indicate a substantial degree of scan induced reorganization. This is somewhat surprising given the degree of crystal perfection seen at the surface of similarly prepared samples (Fig. 2).

3.3. TMDSC of isothermally melt crystallized Vectra®

Representative TMDSC data will be presented first, then effects of annealing time and temperature will be investigated. The TMDSC results are quite different than those for isotropic polymers like PET, possibly because of the weak transitions and subtle effects from reperfection which are more easily detected in polymers like PET. Because

TMDSC is less useful for Vectra®, variable heating rate DSC data were obtained and will be presented in Section 3.4. A 3.5 °C/min TMDSC scan for Vectra® that was melt crystallized at 245 °C for 180 min is shown in Fig. 11. The total heat flow curve displays a melting endotherm with a heat of fusion of 4.1 J/g and a minimum peak temperature of 286 °C. The reversing curve shows a broad very weak endotherm where the heat of fusion is 0.6 J/g and has a peak temperature of 288.3 °C. The NR curve which contains most of the melting has a peak melting temperature of 286.4 °C and a heat of fusion of 3.5 J/g. There is no sign of a recrystallization exotherm in the NR signal and this is quite general for most Vectra® samples. The measured $T_{m,rapid}$ of this sample was 285 °C as described in Section 2. This is illustrated in Fig. 11 and will be discussed in more detail later.

The annealing temperature was increased to 252 °C and TMDSC studies using annealing times of 180 and 1000 min are compared (Fig. 12). The total heat flow (Fig. 12A) for the 180 min sample displays a single endotherm at 294.8 °C with a heat of fusion of 2.6 J/g (Table 1). The reversing data show a very small endotherm of 0.06 J/g with a peak temperature of 298.6 °C (Fig. 12B). The non-reversing curve in Fig. 12C shows an endotherm of 2.54 J/g with a peak temperature of 294.9 °C. The total heat flow curve at 252 °C for 1000 min (Fig. 12A) displays an endothermic peak of 6.5 J/g with a peak temperature of 304.3 °C. The reversing curve also shows a single broad endotherm of

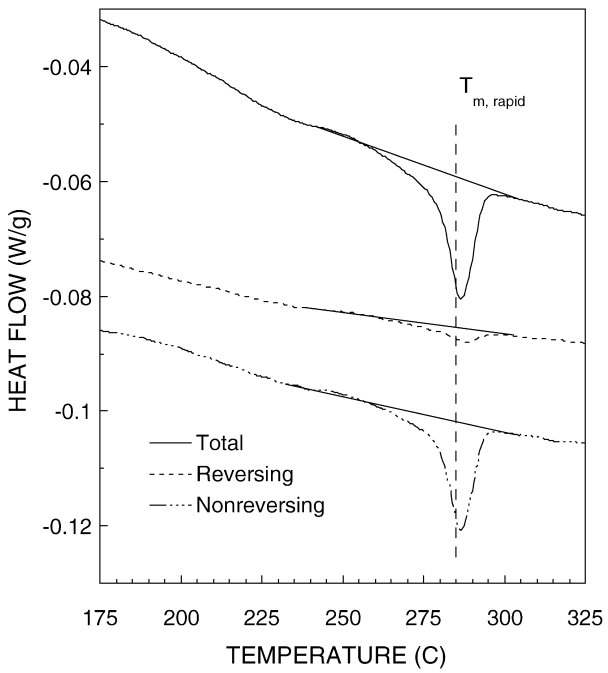

Fig. 11. Total (solid), reversing (dash) and non-reversing (dot-dash) TMDSC curves at 3.5 °C/min for a Vectra® sample melt crystallized at 245 °C for 180 min. Most of the melting is detected in the NR curve. The curves have been shifted vertically for clarity. The rapid heating rate determination of the melting of species originally present equals 285 °C and is indicated by the dashed vertical line.

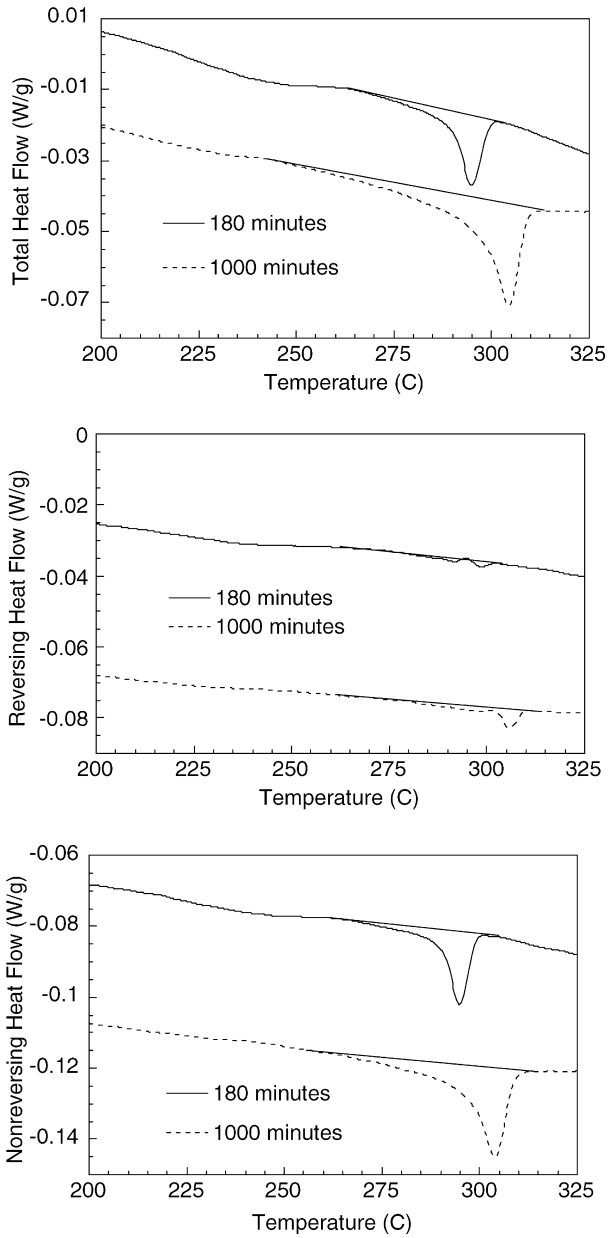

Fig. 12. (A) Total curves of TMDSC data at 3.5 °C/min for a melt crystallized Vectra® sample at 252 °C for 180 (solid) and 1000 min (dashed). The total signal is the sum of the reversing and non-reversing signals and is equivalent to a standard DSC curve. The peak melting temperature increases with annealing time. The curves have been shifted vertically for clarity. (B) Reversing curves at 3.5 °C/min for a melt crystallized Vectra® sample at 252 °C for 180 (solid) and 1000 min (dashed). The curves have been shifted vertically for clarity and the vertical scale has the same magnitude as (A). (C) Non-reversing curves at 3.5 °C/min for a melt crystallized Vectra® sample at 252 °C for 180 (solid) and 1000 min (dashed). Most of the melting is separated into the NR curve. The curves have been shifted vertically for clarity and the vertical scale has the same magnitude as (A).

0.8 J/g with a peak temperature of 305.4 °C in Fig. 12B. Most of the melting occurs in the NR signal with a peak temperature of 303.9 °C and an integrated heat of fusion of 5.7 J/g as seen in Fig. 12C. Comparing the peak melting

Table 1
DSC characterization of melt crystallized Vectra® including total heat of fusion (ΔH)

Sample	Heating rate (°C/min)	T_m (°C)	ΔH (J/g)
245 °C, 180 min	2	292	2.3
245 °C, 180 min	3.5	286	4.1
245 °C, 180 min	10	284	4.1
245 °C, 180 min	20	293	4.2
245 °C, 180 min	40	294	4.4
252 °C, 15 min	3.5	284	1.5
252 °C, 15 min	10	284	1.3
252 °C, 15 min	40	286	1.6
252 °C, 180 min	3.5	295	2.6
252 °C, 180 min	10	297	3.2
252 °C, 180 min	40	302	2.9
252 °C, 1000 min	3.5	304	6.5
252 °C, 1000 min	10	309	6.0
252 °C, 1000 min	40	311	5.6

points (Table 1) of the 180 and 1000 min samples, there is an increase of ~9.5 °C.

3.4. Variable heating rate study of isothermally annealed Vectra®

The results presented above illustrate that TMDSC is unable to characterize DSC scan induced recrystallization in Vectra® except in the region above 285 °C in some samples. This was surprising to us since TMDSC provides excellent characterization of the temperature region of recrystallization in some isotropic polymers [35,38]. To study DSC scan induced reorganization of the melt crystallized samples, a variable heating rate study was performed on the 252 °C melt crystallized samples annealed for 15, 180, and 1000 min (Fig. 13). For the sample annealed for 15 min, the total heat flow curve at 3.5 °C/min displays an endotherm at 284.4 °C followed by a small endotherm at 294.6 °C (Table 1) with a heat of fusion of 1.5 J/g (Fig. 13A). For the 10 °C/min scan, the main endotherm has a peak temperature of 284.1 °C followed by a very small endotherm at 292.5 °C with a heat of fusion of 1.3 J/g. The 40 °C/min scan has as single endotherm at 286.1 °C with a heat of fusion of 1.6 J/g. These data suggest that after 15 min the metastable crystals are prone to scan induced reorganization. At the highest heating rate, the crystals superheat as is indicated by T_m shifting upwards in temperature (Table 1).

For the 180 min sample, an increase in T_m is seen with higher heating rates (Fig. 13B and Table 1). The $T_{m,rapid}$ of this sample was 293 °C as described in Section 2. This is illustrated in Fig. 13B and appears just below the peak melting temperature of the 3.5 °C/min scan suggesting that scan induced perfection is minimal (see Section 4).

For the 1000 min Vectra® sample (Fig. 13C), the peak melting temperature also increases as the heating rate increases (Table 1). This elevation is mainly due to superheating of the crystals. Again, the long time at this

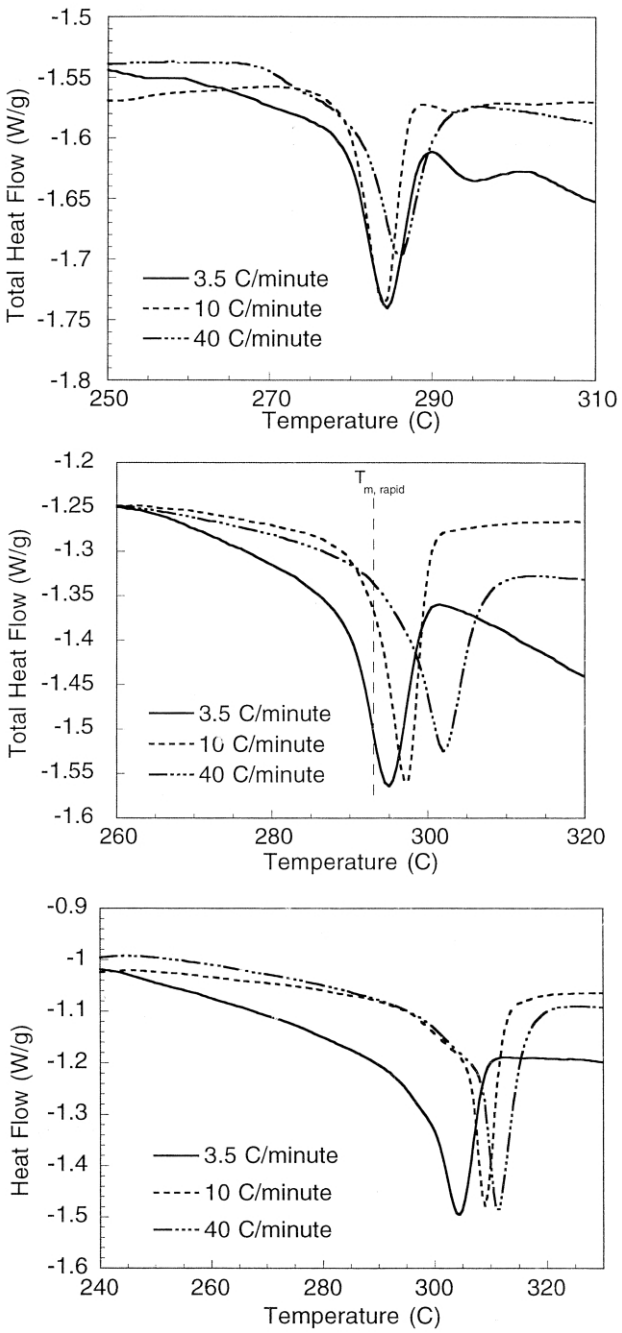

Fig. 13. (A) Standard DSC curves for a Vectra® sample heated at 3.5 (solid), 10 (dashed), and 40 °C/min (dot-dash) after being melt crystallized for 15 min at 252 °C. The vertical axes have been scaled by heating rate. The curves have been slightly shifted vertically for clarity. The peak melting temperature does not shift much with heating rate. (B) Standard DSC curves for a Vectra® sample heated at 3.5 (solid), 10 (dashed), and 40 °C/min (dot-dash) after being melt crystallized for 180 min at 252 °C. The vertical axes have been scaled by heating rate. The curves have been slightly shifted vertically for clarity. The peak melting temperature shifts upward with increasing heating rate. The rapid heating rate determination of the melting of species originally present is $T_{m,rapid} = 293$ °C and is indicated by the dashed vertical line. (C) Standard DSC curves for a Vectra® sample heated at 3.5 (solid), 10 (dashed), and 40 °C/min (dot-dash) after being melt crystallized for 1000 min at 252 °C. The vertical axes have been scaled by heating rate. The curves have been slightly shifted vertically for clarity. The peak melting temperature does shift upwards with faster heating rates.

temperature (252 °C) gives rise to relatively stable crystals which do not undergo a significant amount of DSC scan induced reperfection.

On the other hand, the 180 min Vectra® sample crystallized at 245 °C is a more complicated situation (Fig. 14). The sample was scanned at various heating rates and the peak melting temperatures are listed in Table 1. Also, the $T_{m,rapid}$ of this sample was 285 °C and falls just above the peak melting temperature (284 °C) of the 10 °C/min scan. This suggests that DSC scan induced perfection is minimal at 10 °C/min for this thermal history, but at lower heating rates scan induced perfection occurs (Fig. 14). Evidently the melting point is high at the lowest heating rate because of DSC scan induced perfection (Fig. 14), then at intermediate heating rates reperfection is suppressed because the heating rate is too fast. Finally, at the highest heating rates T_m increases again because of superheating while reperfection is even more suppressed. The TMDSC data for this sample show no evidence of a recrystallization exotherm (Fig. 11).

3.5. Variable heating rate study of lower temperature isothermally annealed Vectra®

The degree of scan induced reperfection is expected to be even higher for lower crystallization temperatures, i.e. lower

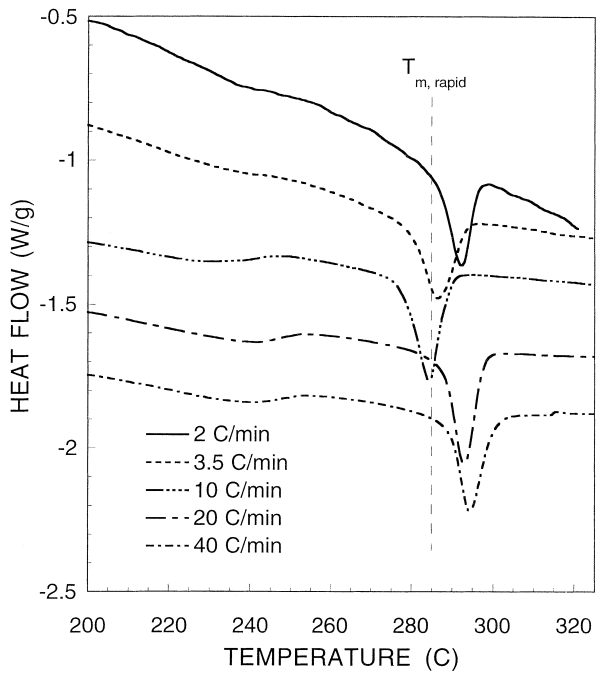

Fig. 14. Standard DSC curves for a Vectra® sample heated at 2 (solid), 3.5 (dashed), 10 (dot-dot-dot-dash), 20 (dot-long dash), and 40 °C/min (dot-short dash) after being melt crystallized for 180 min at 245 °C. The vertical axes have been scaled by heating rate. The curves have been slightly shifted vertically for clarity. The peak melting temperature initially decreases with increasing heating rate up to 10 °C/min and then increases with higher heating rates. The rapid heating rate determination of the melting of species originally present equals 285 °C and is indicated by the dashed vertical line.

degree of crystal stability. For a 5 min, 230 °C annealed sample, at 3.5 °C/min the main endotherm occurs at 281.7 °C with a small endotherm at 297.8 °C and a total heat of fusion of 3.8 J/g (Fig. 15A). At 10 °C/min a single endotherm is detected at 280.7 °C with an integrated heat of fusion of 3.1 J/g. At 50 °C/min, the curve displays a shoulder at 265 °C with the main endotherm at 275.6 °C. The suppression of the highest endotherm strongly suggests that this is due to scan induced recrystallization at the lower heating rates.

The variable heating rate DSC scans for the 180 min sample (230 °C) are given in Fig. 15B. At 3.5 °C/min an endothermic shoulder at 248 °C is detected followed by an endotherm at 280.7 °C with a small endotherm at 298.1 °C. The integrated heat of fusion for the experiment is 5.7 J/g. The 10 °C/min scan shows a dual melting endotherm with peak temperatures of 254.3 and 280.1 °C. The integrated heat of fusion is 6.2 J/g. For the 40 °C/min scan, the major melting endotherm appears at 264 °C with a smaller endotherm at 276.9 °C. The integrated heat of fusion is 6.5 J/g. The low temperature shoulder in the 3.5 °C/min scan (248 °C) appears to increase in temperature and size with heating rate. Conversely, the higher temperature at 280.7 °C endotherm decreases in size and slightly in temperature with increasing heating rate. The weak highest temperature endotherm at 298.1 °C at 3.5 °C/min is absent in the higher heating rates due to less DSC scan induced recrystallization in faster scans.

For the 1080 min sample at 230 °C, experiments were performed at 1, 3.5, 10, and 40 °C/min (Fig. 15C). Each scan displays a single melting endotherm with integrated heats of fusion of 7.2, 7.3, 7.3, and 7.5 J/g, respectively. The peak melting temperatures with increasing heating rate are 284.1, 279.9, 278.2, and 282.6 °C. The peak temperature decreases from the 1 to 10 °C/min scans indicating a decrease in the amount of DSC scan induced reperfection. The 40 °C/min scan shows an increase in peak temperature which results from superheating at this higher heating rate and a suppression of reperfection. Fig. 15C shows that $T_{m,rapid}$ = 280 °C, and this quantity is about the same as the peak melting temperature of the 3.5 °C/min scan suggesting that scan induced perfection is limited at heating rates above this (see Section 4).

3.6. Annealing time dependence of isothermally annealed Vectra®

The next series of samples were prepared at a lower isothermal temperature of 230 °C using annealing times of 5, 180, and 1080 min. The 5 min sample was prepared by first melting the sample at 340 °C in the DSC cell and then cooling rapidly (20 °C/min) to 230 °C. After holding isothermally for 5 min, the DSC cooled the sample at 10 °C/min to 200 °C before the TMDSC heating scan. The longer time annealed samples were prepared by melt crystallization in a temperature controlled oven (see Section 2). These TMDSC scans were

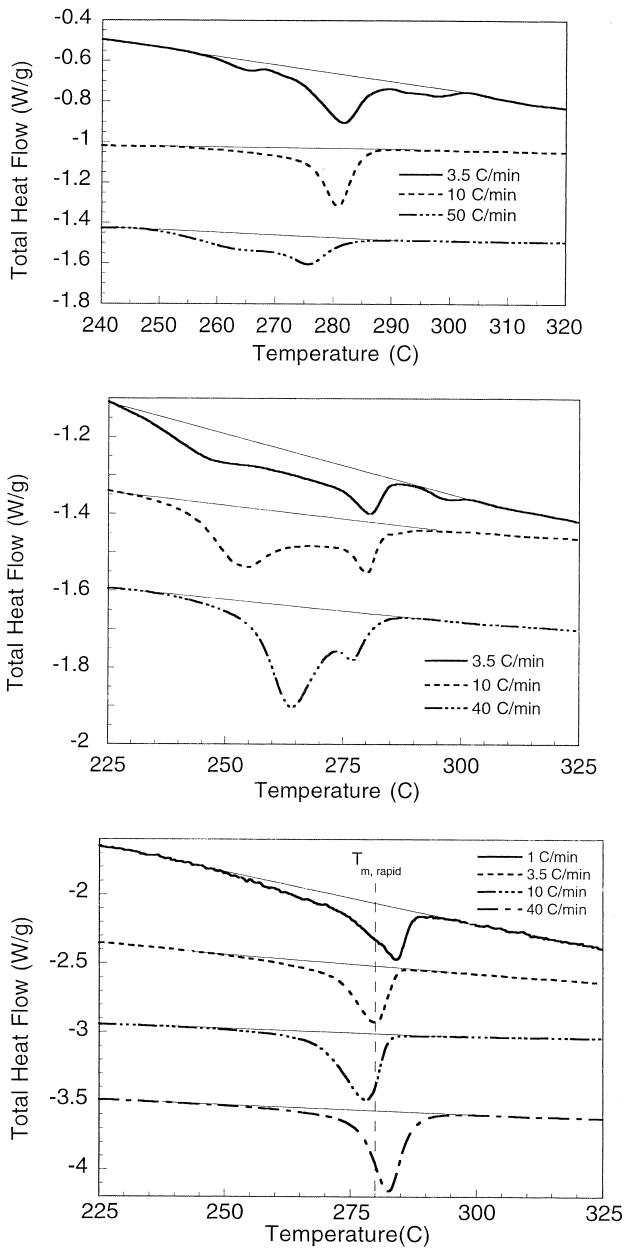

Fig. 15. 15A Standard DSC curves for a Vectra® sample heated at 3.5 (solid), 10 (dashed), and 50 °C/min (dot-dash) after being melt crystallized in a DSC experiment for 5 min at 230 °C. The vertical axes have been scaled by heating rate. The curves have been slightly shifted vertically for clarity. The peak melting temperature decreases with increasing heating rate. (B) Standard DSC curves for a Vectra® sample heated at 3.5 (solid), 10 (dashed), and 40 °C/min (dot-dash) after being melt crystallized for 180 min at 230 °C. The vertical axes have been scaled by heating rate. The curves have been slightly shifted vertically for clarity. The peak melting temperature of the lower endotherm shifts upward with increasing heating rate. The higher endotherm peak melting temperature decreases with increasing heating rate. (C) Standard DSC curves for a Vectra® sample heated at 1 (solid), 3.5 (dashed), 10 (dot-dot-dot-dash), and 40 °C/min (dot-dash) after being melt crystallized for 1080 min at 230 °C. The vertical axes have been scaled by heating rate. The curves have been slightly shifted vertically for clarity. The rapid heating rate determination of the melting of species originally present equals 280 °C and is indicated by the dashed vertical line. The peak melting temperature initially decreases with increasing heating rate up to 10 °C/min and then increases with the higher heating rate.

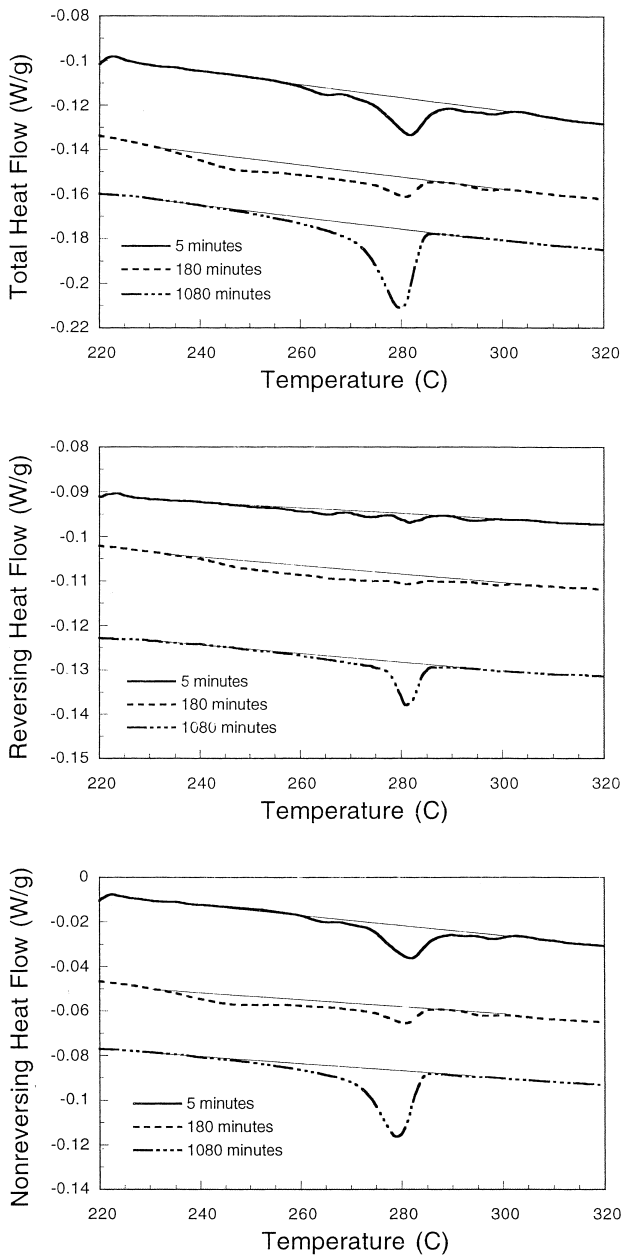

Fig. 16. (A) Total curves of TMDSC data at 3.5 °C/min for a melt crystallized Vectra® sample at 230 °C for 5 (solid), 180 (dashed), and 1080 min (dot-dash). The curves have been shifted vertically for clarity. (B) Corresponding reversing curves of TMDSC data at 3.5 °C/min for a melt crystallized Vectra® sample at 230 °C for 5 (solid), 180 (dashed), and 1080 min (dot-dash). The curves have been shifted vertically for clarity. The vertical scale is one-half of the total and non-reversing scales to enhance visualization of the features. (C) Corresponding non-reversing curves of TMDSC data at 3.5 °C/min for a melt crystallized Vectra® sample at 230 °C for 5 (solid), 180 (dashed), and 1080 min (dot-dash). The curves have been shifted vertically for clarity and the vertical axis has the same magnitude as (A).

started at room temperature and the modulated runs are shown in Fig. 16. For the 5 min sample, the total heat flow (Fig. 16A) displays a small endothermic peak at 265.7 °C, followed by a large endotherm at 281.7 °C, and finally a small endotherm at 297.8 °C. The heat of fusion is 3.8 J/g. The reversing curve (Fig. 16B) for the sample shows a broad endotherm with a peak melting temperature of 281.6 °C and a heat of fusion of 0.7 J/g. The NR curve (Fig. 16C) displays a shoulder at 265.7 °C followed by a broad endotherm at 281.7 °C and a small endotherm at 298.5 °C. The heat of fusion for the NR curve is 3.1 J/g.

After 180 min at 230 °C, the total heat flow displays a shoulder at 248 °C, followed by an endotherm at 280.7 °C with a small endotherm at 298.1 °C (Fig. 16A). The heat of fusion is 5.8 J/g. The reversing curve in Fig. 16B shows a broad endotherm of 1.9 J/g with a peak temperature of 281.1 °C. The NR curve (Fig. 16C) shows a shoulder at 250 °C followed by an endotherm at 280.3 °C with a small endotherm at 297.3 °C. This curve has a heat of fusion of 3.9 J/g.

After 1080 min at 230 °C, the total heat flow shown in Fig. 16A displays a broad endotherm of 7.3 J/g with a peak temperature at 279.9 °C. The reversing curve (Fig. 16B) displays an endotherm at 280.9 °C with a heat of fusion of 3 J/g. The NR curve in Fig. 16C also has a single endotherm at 278.9 °C and its heat of fusion is 4.3 J/g.

In order to more fully understand the influence of annealing time and DSC heating rate on morphological development at 230 °C, the total heat flows of the three different annealing times of 5, 180, and 1080 min are presented in Fig. 16A. At 3.5 °C/min after 5 min of annealing, a small endothermic peak occurs at 265.7 °C, followed by the main melting endotherm at 281.7 °C, and then a small endotherm at 297.8 °C. The total heat of fusion for this sample is 3.8 J/g. After 180 min at 230 °C, the curve displays a broad shoulder at 248 °C, an endotherm at 280.7 °C, followed by a small endotherm at 298.1 °C. The integrated heat of fusion after 180 min increases to 5.75 J/g. When the annealing time is increased to 1080 min, the total heat flow for the 3.5 °C/min scan displays a single endotherm at 279.9 °C. The heat of fusion has increased to 7.3 J/g. The crystallinity of the Vectra® sample has increased with annealing time as has the stability of the crystals. At 10 °C/min, the total heat flows for the same three annealing times at 230 °C (Fig. 17) show similar trends to the data at 3.5 °C/min (Fig. 15A). The contributions of melting and recrystallization are complex and will be discussed in Section 4.

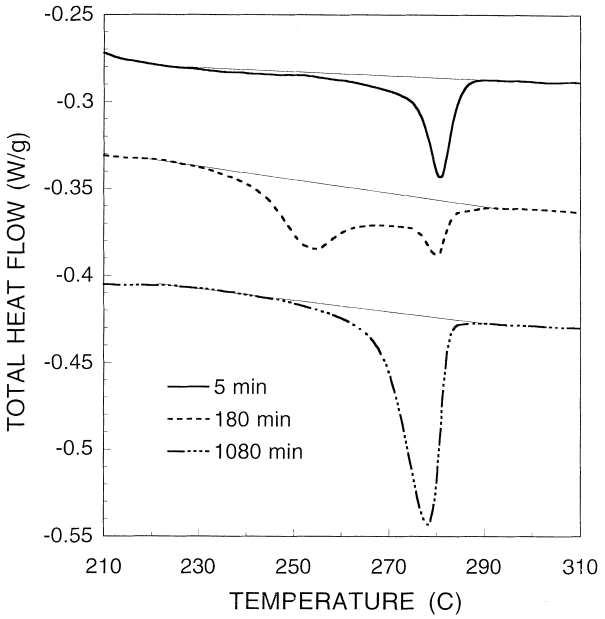

Fig. 17. Standard DSC curves at 10 °C/min for a melt crystallized Vectra® sample at 230 °C for 5 (solid), 180 (dashed), and 1080 min (dot-dash). The curves have been shifted vertically for clarity.

4. Discussion

AFM provides high resolution characterization of morphology in oriented filaments before (Fig. 1) and after annealing (Figs. 2 and 3). The lamellae in the annealed samples have the expected orientation [9–17] with their long direction perpendicular to the fiber direction. Similar oriented lamellae were seen by SEM in oriented and annealed samples of low MW HBA/HNA copolymer [17], and the degree of perfection seen by AFM before and after annealing is consistent with the WAXD characterization [1,6,9,17,18]. SAXS characterization also showed a distinct long period in the meridianol scattering direction [17,18] which is consistent with the AFM characterization of the orientation and spacing between lamellae (Figs. 2 and 3). Several TEM studies also characterized this long period between lamellae in the meridian direction, and TEM of etched surfaces shows continuous lamellae about 10 nm thick and 100 nm long oriented with their length perpendicular to the orientation direction [9,17]. Previous studies of melt extruded oriented Vectra® A950 films also characterized the macro-fibrillar structure of the surface in addition to atomic resolution of the lamellae [45]. AFM also provides some additional preliminary characterization of the components of the lamellae. It is seen that most lamellae are comprised of multiple smaller crystallites, at least from the AFM surface characterization. These are stacked together to give what is referred to as lamellae. These small crystallites are approximately 10 nm thick and 15 nm long in the oriented sample (Fig. 2). Possibly similar phenomena have been reported in other semi-crystalline polymers [46]. Related blocky lamellae in Vectra® crystallized from a non-oriented melt during non-isothermal cooling contain crystallites 7 nm thick and 20 nm long (Fig. 4), and in these non-oriented samples larger lamellae form because of much lower degrees of nucleation. Although spherulitic growth out of a nematic melt of relatively rigid chains probably cannot occur because of the

nematic chain orientation and non-chain folding nature of these copolymers, one can still consider that nucleation of lamellae will partially govern morphology. This nucleation depends on degree of undercooling as is true for most polymers.

AFM suggests that part of the secondary crystallization or slow perfection consists of coalescence of smaller crystals combined with further chain addition and registration of crystallizable units in lamellae (compare Figs. 1 and 2). In less nucleated samples (Fig. 5), regions that were not initially crystallized may also exist depending on the thermal history because of the random copolymer nature of Vectra®. AFM characterized the very imperfect lamellar morphology resulting from quenching.

Increasing the melt crystallization time from 10 to 130 min at 252 °C caused an infilling of new lamellae several hundred nanometers long between existing ones, and the only other change in dimension detected was the thickness of the lamellae in the direction perpendicular to the long dimension. This thickness increased from 24 to 35 nm, respectively. A non-isothermally crystallized Vectra® sample formed by cooling from the melt at 20 °C/min contained smaller and more densely packed lamellae than a 252 °C isothermally melt crystallized sample presumably due to a larger degree of undercooling in the former. In all Vectra® systems including mechanically oriented and annealed ones, lamellae were found to consist of thinner stacks of crystallites with thicknesses on the order of 10 nm. It is not known whether this contrast of the very small crystallites is due to AFM surface sensitivity, or whether the lamellae are actually continuous under the surface.

4.1. TMDSC of azomethine LCPs

The LCPs studied here exhibited a wide range of thermal responses spanning recrystallization phenomena in the azomethine LCP more typical of common polymers like PET, [11,32,35,38] to unusual and sometimes complicated thermal behavior of Vectra®. The azomethine LCP is a homopolymer and exhibits cold crystallization, recrystallization into polymorphic forms, followed by multiple melting of various recrystallized species. There are some similarities to other semi-crystalline isotropic polymer systems [47]. Variable heating rate DSC confirms that DSC scan induced recrystallization including polymorphic transformations [47] dominates the region between 80 and 170 °C (Fig. 7). The NR signal of TMDSC (Fig. 7) for the azomethine LCP provides excellent resolution of the exothermic events associated with cold crystallization at 90 °C and polymorphic crystal transformations which have recently been studied by standard DSC in polyamides [47]. Related melting and recrystallization of metastable crystals in isotropic polymers like PET [35,38] are also characterized with better detail by TMDSC than DSC. The nematic-to- isotropic transition at 309 °C in azomethine (Fig. 7) is obviously an event not seen in isotropic polymers, and was discussed in the Section 3.

4.2. Non-isothermally crystallized Vectra®

While the azomethine LCP is a homopolymer, Vectra® is a 'random' copolymer. The crystallization from the melt is rapid and suggests that cocrystallization of the comonomers takes place [1,7–9,16,22]. The metastability of the crystals that form under non-isothermal or relatively low temperature isothermal annealing conditions has been briefly discussed [2,20]. Much of the work presented below will show that the ~280 °C endotherm measured by DSC and TMDSC for short time annealed samples, can actually be attributed to DSC scan induced crystal perfection. This partly resolves the controversy discussed by Cheng et al. [20] and later reviewed by Langelaan and de Boor [16]. In many isothermally crystallized random copolyester compositions including Vectra®, the '280 °C endotherm' associated with the rapid crystallization step after short annealing times (T_{anneal} ~ 230 °C), actually has a higher T_m than samples annealed at intermediate times at the same temperature [2,16,20]. A different degree of orientation and thus a different entropy of melting was offered as one explanation for the surprisingly elevated T_m at short times given the known low degree of crystal perfection of the short time annealed samples [20]. Another explanation verified below is that the apparent high T_m for the short time annealed and related samples is a consequence of DSC scan induced crystal perfection or melting and recrystallization. In this study TMDSC, variable heating rate DSC, and other techniques not used earlier have been applied here to address these issues.

TMDSC and DSC on non-isothermally crystallized and sometimes isothermally crystallized Vectra® generally show three endothermic regions around 230, 280 and 295 °C (Fig. 9). The highest temperature endotherm is probably the easiest to explain. It is present only in initially 'poorly' crystallized samples giving a morphology amenable for melting and recrystallization during slow DSC heating leading to the formation of this high melting fraction. The small exotherm at 287 °C in the NR curve in Fig. 9 is direct evidence of recrystallization. Also supporting this are elevated heating rate DSC data where the high melting fraction corresponding to the 295 °C endotherm is suppressed due to slow recrystallization kinetics (Fig. 10). The high melting species have been extensively studied by others [3,4]. Finally, melt crystallization under appropriate conditions such as 230 °C for 1080 min (Fig. 15C) and several other thermal histories suppresses the ~295 °C endotherm. This is because the crystals formed are stable enough during DSC heating that by the time they melt the insufficient undercooling prohibits recrystallization.

Interpretation of the 230 and 280 °C regions has similarities to many of the melt crystallized Vectra® samples discussed below. These regions are deceptive

because of DSC scan-induced crystal perfection. The reperfection can be substantially faster than in polymers like PET making it difficult to detect and quantify in Vectra®. The region below 280 °C in the non-isothermally crystallized sample is characterized by both R and NR endothermic melting (Fig. 9), but no NR exothermic behavior is seen below 280 °C even though this 280 °C endotherm will be shown to have a dominant contribution from DSC induced perfection in the non-isothermally crystallized sample. Higher heating rate data for the unannealed non-isothermally crystallized sample show a slight drop in T_m in Fig. 10 suggesting a reperfection contribution. Evidence is also seen in Fig. 15A and B for the short time 230 °C isothermally crystallized samples where upon extrapolation to higher heating rates, the 280 °C endotherm shifts to lower temperatures and approximately begins to disappear. Final verification is obtained from independent rapid heating rate melting point determinations, where the non-isothermally crystallized sample is completely liquified and melted by 260 ± 3 °C when heated at ~1000 °C/s! (Fig. 9) This $T_{m,rapid} = 260$ °C is indicated on the figure, and is substantially below the 280 °C endotherm which proves that the latter is almost entirely due to scan induced recrystallization. This illustrates how deceptive DSC data are for such samples. Regardless of DSC induced recrystallization, the total enthalpies of fusion used to characterize kinetics of crystallization in several previous studies are correct [2,16,19,20].

Annealing the non-isothermally crystallized sample from the glass at 230 °C for 180 min (Fig. 10) sharpens both lower transitions and diminishes the 295 °C transition because increased perfection gives less chance for melting and recrystallization. Shorter 230 °C anneals give similar trends and any anneal at 230 °C generally reduces the endotherm at temperatures below the annealing temperature because those metastable crystals are melted and perfected. The oriented sample studied by AFM that was cold crystallized at 230 °C (Fig. 2) also shows some metastability with a small recrystallization endotherm at 295 °C (Fig. 10). Oriented systems are highly nucleated when first crystallized and this can increase the degree of metastability.

4.3. Isothermally melt crystallized Vectra®

Although isothermal melt crystallization leads to a single endotherm in many Vectra® samples, this endotherm can be deceptively complex. Fig. 14 for example gives data for an intermediate temperature and time melt crystallized sample (245 °C for 180 min), and the elevation of T_m at low DSC heating rates suggests that scan induced reperfection is taking place. This reperfection is eventually suppressed by higher heating rates where T_m finally begins to rise due to superheating effects. The minimum in T_m is around 10 °C/min. Scan induced reperfection is also verified by independently measured melting points of the initially present primary crystals by the rapid heating rate technique. For example, the rapid heating rate melting point [33] ($T_{m,rapid}$) of Vectra® annealed for 180 min at 245 °C is equal to 285 °C which is consistent with the melting point determined by DSC at 10 °C/min of 283 °C (Fig. 14).

Many other examples were presented here where the melting point decreased initially with increasing heating rate due to scan induced perfection. Long annealing times, especially at higher temperatures, produced samples which did not exhibit this behavior suggesting that the crystals were less metastable and that they were not perfected by the DSC scan. Examples include Fig. 13B and C where the samples were annealed at 252 °C for 180 and 1000 min, respectively. These conditions lead to relatively high melting crystals consistent with previous DSC results which have also characterized the progression to higher melting points [2,4,7,16,19,20]. $T_{m,rapid}$ for the 252 °C (180 min) annealed sample is 293 ± 5 °C and is consistent with the DSC melting point (Figs. 12 and 13B). At moderate annealing temperatures (230 °C), even 1080 min is insufficient to provide entirely stable crystals. For example, variable heating rate DSC (Fig. 15C) shows evidence for reperfection in this case at the lowest heating rates. The degree of reperfection is small. This is proven by the value of $T_{m,rapid} = 280$ °C which is essentially the same as T_m from the 10 °C/min DSC heating scan (Fig. 15C). Apparently, lower heating rates induce a small degree of crystal perfection as is indicated by the higher T_m at 3.5 °C/min heating rates (Fig. 15C).

Fig. 12 is an example of the well known effect [2,4,7,16,19,20] of increasing crystal perfection in LCPs like Vectra® with longer annealing times during melt crystallization. Here, T_m is seen to increase substantially due to the 252 °C annealing. Although the endotherms in Vectra® are generally dominated by the NR contributions except maybe for the non-isothermally crystallized samples (Fig. 9), the data for the high temperature annealed samples in Fig. 12 are almost completely NR. This has some similarities to high temperature annealed (solid state polymerized) PET where the superheating necessarily causes the high non-reversing component [11,33,36] (see Section 2). It is likely that transesterification in Vectra® at 252 °C is mainly responsible for the increase in T_m in Fig. 12 [4,19]. These chemical interchange reactions allow chains to 'avoid' chain diffusional barriers, and thus crystallizable units can recombine in more optimal conformations. Such crystallization and recrystallization occurs over the time scale of the chemical interchange reactions.

Evidence from variable heating rate DSC suggests that the 280 °C endotherm for moderately annealed samples is influenced by scan induced crystal reperfection. Normally for polymers like azomethine (Fig. 7), PET [11,35,38], etc. the TMDSC NR signal detects exothermic recrystallization over broad temperature ranges. A higher temperature NR exothermic response at ~285 °C is only seen in Vectra® samples with the highest degree of crystal metastability (Figs. 9, 10 and 15). This small exotherm is a signature of

one form of high temperature recrystallization and eventually contributes to the small 295 °C endotherm in these figures for these initially poorly crystallized samples. Several examples of variable heating rate DSC proved that slow heating rates lead to crystal perfection causing the occurrence of the 280 °C 'endotherm' region to be sometimes completely scan induced even though no NR exotherm is seen below 280 °C. The independent rapid heating rate melting point technique showed for example that the non-isothermal crystallized sample with a DSC melting point of 280 °C really had a melting point around 260 ± 3 °C when heated at ~1000 °C/s! (i.e. $T_{m,rapid}$ = 260 °C in Fig. 9) This is substantially below the 280 °C endotherm which proves that the latter is almost entirely due to scan induced recrystallization. We call this perfection rather than recrystallization since we cannot detect a NR exotherm between 250 and 280 °C where we might expect it.

We have a few possibilities of why no NR exotherm is detected between 250 and 280 °C by TMDSC in Vectra®. It is possible that reperfection occurs with such a small exothermic signal that it is too weak to detect [14]. It is also possible that melting is different in Vectra® compared to PET because it is dominated by the NR component even for 'poorly crystallized' samples. Thus, any exothermic contribution may have been overwhelmed and therefore compensated by the NR endothermic signal in the critical region between 250 and 280 °C.

We must also explain the difference between Vectra® and other polymers like PET where a large NR melting contribution is seen in Vectra® in a situation where metastable crystals exist. Under such conditions PET exhibits a large reversing endothermic contribution in the broad melting region [35,38]. After long time high temperature annealling (solid state polymerization) of PET, the high melting crystals which are formed may have some similarity with those formed in Vectra® after only short annealing times. The similarities could include the nature of the conformation of the chains in the 'network' in Vectra® [9], compared to the increasing levels of amorphous tie chains which possibly evolve during the solid state polymerization of PET [11,35,48]. The change in entropy of melting due to the conformation of the tie chains in PET was proposed as an explanation for the increase in T_m at constant or even *decreasing* lamellar thickness during solid state polymerization [11,48]. Because the amorphous conformations must relax for melting to occur, these type of morphologies including those in Vectra® (crystals from both fast and slow steps) exhibit superheating characteristics. Any crystal which superheats will contribute to a large NR endothermic signal [35,38]. This could explain the TMDSC results for Vectra® where in general the melting for most annealing conditions including non-isothermal crystallization, is dominated by the NR component.

5. Conclusions

DSC is widely used to study evolution of secondary crystal development in isotropic homopolymers. In these systems a secondary 'low' temperature endotherm evolves and is detected a few degrees above the isothermal annealing temperature and is known to exhibit a slow increase in size and peak melting temperature [10–12,35,38]. Melting of separate species presumably contribute in this case, where the primary crystals with a higher degree of perfection melt at higher temperatures. In LCPs, because of the rapid establishment of a physical cross-linked network during the primary crystallization stage, [2,9] secondary crystallization is more appropriately discussed in terms of a perfection process [2,7–9]. Unfortunately, the study of this perfection process in Vectra® by thermal methods is hindered by DSC scan induced recrystallization, especially for the short time annealed samples.

AFM suggests that part of the secondary crystallization or slow perfection consists of coalescence of smaller crystals combined with further chain addition and registration of crystallizable units in lamellae (compare Figs. 1 and 2). In non-oriented Vectra®, regions which were not initially crystallized may also exist depending on the thermal history (Fig. 5), because of the random copolymer nature of Vectra®. AFM was used in this study to characterize the very imperfect lamellar morphology resulting from quenching, which then evolved to relatively well developed lamellae after elevated temperature isothermal crystallization. A non-isothermally crystallized Vectra® sample formed by cooling from the melt at 20 °C/min (Fig. 4) contained smaller and more densely packed lamellae than a 252 °C isothermally melt crystallized sample (Fig. 6) presumably due to a larger degree of undercooling during crystallization in the former.

Increasing the melt crystallization time from 10 to 130 min at 252 °C caused an infilling of new lamellae several hundred nanometers long between existing ones, and the only other change in dimension detected was the thickness of the lamellae in the direction perpendicular to the long dimension. This thickness increased from 24 to 35 nm, respectively. In all Vectra® systems including mechanically oriented and annealed ones, lamellae were found to consist of stacks of very small crystallites with thicknesses on the order of 10–15 nm. It is not known whether this contrast detecting very small crystallites is due to AFM surface sensitivity, or whether the lamellae are actually continuous under the surface.

A variety of crystallization conditions lead to metastable crystal morphologies in Vectra® prone to DSC scan induced perfection and sometimes melting and recrystallization. For the typical non-isothermally crystallized or lower temperature isothermally crystallized sample, DSC scan induced crystal perfection is a complication in comparing with non-destructive techniques like AFM. The largest amount of reperfection is known to occur at the

slowest heating rates as is true for Vectra®. The scan induced perfection is verified by variable heating rate DSC and independently measured melting points of the initially present primary crystals using the rapid heating rate technique described here. It takes fairly high melt crystallization temperatures to improve the crystal stability in Vectra®. Long time, high temperature annealing leads to increased melting points that are partly a result of chemical interchange reactions. The DSC and TMDSC data characterize these superheatable high melting crystals, and show some similarities with high temperature annealed PET where superheating is also detected by DSC and TMDSC.

TMDSC characterization of Vectra® is also shown to be substantially different than that for typical isotropic polymers such as PET and even the azomethine homopolymer LCP studied here. Metastable morphologies in these typical polymers give rise to broad and strong NR recrystallization exotherms, while in Vectra® NR exotherms are rarely detected. Several examples of variable heating rate DSC proved that slow heating rates lead to crystal perfection causing the 280 °C 'endotherm' region to be sometimes completely scan induced even though no NR exotherm is seen below 280 °C. The independent rapid heating rate melting point technique showed for example that the non-isothermal crystallized sample with a DSC melting point of 280 °C really had a melting point around 260 ± 3 °C when heated at ~1000 °C/s! (i.e. $T_{m,rapid}$ = 260 °C in Fig. 9) This is substantially below the 280 °C endotherm which proves that the latter is almost entirely due to scan induced recrystallization. Similar results of metastability are found for samples melt crystallized for a few minutes at 230 °C. Other annealing conditions, especially higher temperatures and longer times, lead to more stable morphologies where $T_{m,rapid}$ is approximately equal to the DSC or TMDSC peak melting temperature.

Acknowledgements

We thank Dr B. Wood of DuPont for helpful comments.

References

[1] Butzbach GD, Wendorff JH, Zimmermann HJ. Polymer 1986;27:1337.
[2] Cheng SZD. Macromolecules 1988;21:2475.
[3] Lin YG, Winter HH. Macromolecules 1991;24:2877.
[4] Kachidza J, Serpe G, Economy J. Makromol Chem, Macromol Symp 1992;53:65.
[5] Chung TS, Calundann GW, East AJ, Encyclopedia of engineering materials, vol. 2. New York: Marcel Dekker; 1989. p. 625.
[6] Kaito A, Kyotani M, Nakayama K. Macromolecules 1990;23:1035.
[7] Löffler R, Navard P. Macromolecules 1992;25:7172.
[8] Dainelli D, Chapoy LL. Macromolecules 1993;26:385.
[9] Hudson SD, Lovinger AJ. Polymer 1993;34:1123.
[10] Marand H, Alizadeh A, Farmer R, Desai R, Velikov V. Macromolecules 2000;33:3392.
[11] Wang ZG, Hsiao BS, Sauer BB, Kampert WG. Polymer 1999;40:4615.
[12] Lee Y, Porter RS. Macromolecules 1987;20:1336.
[13] Cheng SZD, Cao M-Y, Wunderlich B. Macromolecules 1986;19:1868.
[14] Blundell DJ, Buckingham KA. Polymer 1982;23:359.
[15] Cao M-Y, Wunderlich B. J Polym Sci, Polym Phys Ed 1985;23:521.
[16] Langelaan HC, Posthuma de Boer A. Polymer 1996;37:5667.
[17] Hanna S, Lemmon TJ, Spontak RJ, Windle AH. Polymer 1992;33:3.
[18] Wilson DJ, Vonk CG, Windle AH. Polymer 1993;34:227.
[19] Chung T-S, Cheng M, Goh SH, Jaffe M, Calundann GW. J Appl Polym Sci 1999;72:1139.
[20] Cheng SZD, Janimak JJ, Zhang A, Zhou Z. Macromolecules 1989;22:4240.
[21] Sauer BB, Beckerbauer R, Wang L. J Polym Sci, Polym Phys 1993;31:1861.
[22] Biswas A, Blackwell J. Macromolecules 1988;21:3152.
[23] Flores A, Ania F, Balta Calleja FJ, Ward IM. Polymer 1993;34:2915.
[24] Cheng SZD, Zhang A, Johnson RL, Wu Z, Wu HH. Macromolecules 1990;23:1196.
[25] Cheng SZD, Johnson RL, Wu Z, Wu HH. Macromolecules 1991;24:150.
[26] Johnson RL, Cheng SZD. Macromolecules 1993;26:94.
[27] Chen W, Toda A, Wunderlich B. In: Williams KR, editor. Proceedings of the 26th NATAS Conference, Cleveland, OH, vol. 26.; 1998. p. 157–62.
[28] Chen W, Dadmun M, Zhang G, Boller A, Wunderlich B. Thermochim Acta 1998;324:87.
[29] Biswas A, Gardner KH, Wojtkowski PW. Liquid crystalline polymers. In: Weiss RA, Ober CK, editors. ACS symposium series 435. Washington, DC: American Chemical Society; 1990.
[30] TMDSC compendium, T.A. Instruments, Inc., 109 Lukens Drive, New Castle, DE 19720
[31] Software from T.A. Instruments, Inc., 109 Lukens Drive, New Castle, DE 19720
[32] Sauer BB, Kampert WG, Blanchard EN, Threefoot SA, Hsiao BS. Polymer 2000;41:1099.
[33] Merzlyakov M, Schick C. Thermochim Acta 1999;330:55.
[34] Toda A, Tomita C, Hikosaka M, Saruyama Y. Polymer 1998;39:5093. Toda A, Tomita C, Hikosaka M. J Therm Anal Cal 1998;54:623.
[35] Sauer BB, Kampert WG, McLean RS, Carcia PF. J Therm Anal Cal 2000;59:227.
[36] Kampert WG, Sauer BB. Polym Engng Sci 2001;41:1714.
[37] Thomas LT. Personal communication
[38] Kampert WG, Sauer BB. Polymer 2001;42:8703.
[39] Reading M. Trends Polym Sci 1993;8:248.
[40] Okazaki I, Wunderlich B. Macromol Rapid Commun 1997;18:313.
[41] Okazaki I, Wunderlich B. Macromolecules 1997;30:1758.
[42] McLean RS, Sauer BB. J Polym Sci, Polym Phys 1999;37:859.
[43] Magonov SN, Elings V, Whangbo M-H. Surf Sci Lett 1997;385:375.
[44] McLean RS, Sauer BB. Macromolecules 1997;30:8314.
[45] Gould SAC, Shulman JB, Schiraldi DA, Occelli ML. J Appl Polym Sci 1999;74:2243.
[46] Heck B, Hugel T, Iilima M, Sadiko E, Strobl G. New J Phys 1999;1:17.1.
[47] Starkweather HW, Avakian P, Gardner KH, Hsiao BS, Keating MY, Ng H. J Therm Anal Cal 2000;59:519.
[48] Zachmann HG, Schmidt GF. Makromol Chem 1962;52:23.